REGULAR ARTICLE

blood neoplasia

Mezigdomide combined with bortezomib disrupts the cell cycle and elicits superior antitumor effects in multiple myeloma

Chad C. Bjorklund,[1] Marta Larrayoz,[2] Jian Kang,[1] Hsiling Chiu,[1] Natasha Shtraizent,[1] Lei Wu,[1] Shirong Li,[1] Chih-Chao Hsu,[1] Junfei Zhao,[1] Michael Amatangelo,[1] Tracy T. Chow,[1] Krista Wollerman,[1] Ram Kumar Singh,[3] Sneha Sridhara,[3] Shailesh Dudhgaonkar,[4] Prakash Subramanyam,[3] Kaushik Ghosh,[4] Paul G. Richardson,[5] Nizar J. Bahlis,[6] Anjan Thakurta,[1,7] Jose A. Martinez-Climent,[2] Anita K. Gandhi,[1] and Patrick R. Hagner[1]

[1]Bristol Myers Squibb, Translational Development, Summit, NJ; [2]Center for Applied Medical Research CIMA, Cancer Center University of Navarra, Navarra Institute for Health Research (IDISNA), Centro de Investigation Biomedica en Red (CIBERONC), Pamplona, Spain; [3]Biocon Bristol Myers Squibb, Research and Development Centre, Syngene International Ltd, Bangalore, India; [4]Bristol Myers Squibb, Research and Development, Bangalore, India; [5]Dana-Farber Cancer Institute, Jerome Lipper Multiple Myeloma Center, Boston, MA; [6]Arnie Charbonneau Cancer Institute, Cumming School of Medicine, Department of Oncology, University of Calgary, Calgary, AB, Canada; and [7]Radcliffe Department of Medicine, University of Oxford, Oxford, United Kingdom

Key Points

- The combination of MEZI with BTZ increases cell death through disruption of the cell cycle.
- The combination of MEZI/BTZ/DEX demonstrates superior efficacy compared with POM/BTZ/DEX in the preclinical setting.

Triplet regimens that include an immunomodulatory agent, proteasome inhibitor, and dexamethasone are widely used in newly diagnosed and relapsed/refractory (R/R) multiple myeloma (MM). Mezigdomide (MEZI; CC-92480) is a cereblon E3 ubiquitin ligase modulator that is being clinically investigated in combination with bortezomib (BTZ) and low-dose dexamethasone (DEX) for safety and efficacy in pretreated R/RMM. The single-agent mechanism of action (MOA) of MEZI has been defined by the recruitment and degradation of essential MM transcription factors Ikaros and Aiolos, leading to cell autonomous antitumor effects and immune modulation. These effects were confirmed in patients based on pharmacodynamic measurements of Ikaros/Aiolos degradation in biomarker evaluations of immune subsets. However, the MOA of triplet regimens, including that of MEZI/BTZ/DEX remain poorly defined. To better understand the MOA of this triplet combination, we compared the mechanistic contributions of MEZI, BTZ, or DEX alone, or in combination, in preclinical MM models in vitro and in vivo. Additionally, we have compared these results with similar combinations with the immunomodulatory agent pomalidomide (POM). Our studies indicate that the MEZI/BTZ/DEX triplet is superior to all single agents and POM/BTZ/DEX in terms of potency of antiproliferative and proapoptotic activities, substrate degradation depth and kinetics in the presence of BTZ, and in vivo efficacy. We show that the combination of MEZI with BTZ increases cell death through disruption of multiple phases of the cell cycle and this thereby enhances the direct cytotoxic effects of the combination treatment.

Introduction

Mezigdomide (MEZI; CC-92480) is a novel, potent cereblon (CRBN) E3 ubiquitin ligase modulator (CELMoD) agent being investigated in patients with relapsed/refractory (R/R) multiple myeloma (MM).[1,2] The treatment landscape for MM has undergone a transformation with the introduction of high-dose therapy followed by stem cell transplant, proteasome inhibitors (PIs), immunomodulatory

Submitted 2 December 2024; accepted 29 September 2025; prepublished online 7 November 2025. https://doi.org/10.1016/j.bneo.2025.100179.

Original data are available from the corresponding author, Chad C. Bjorklund (chad.bjorklund@bms.com), on request.

The full-text version of this article contains a data supplement.

agents (IMiDs), monoclonal and bispecific antibodies, and chimeric antigen receptor T-cell therapies.[1,3-9] Triplet combination regimens (IMiD, PI, and corticosteroid) have become a standard of care in both newly diagnosed MM and R/RMM settings. The availability of multiple agents with complementary and distinct mechanisms of action (MOA) have made combining treatments an attractive strategy to circumvent or overcome mechanisms of resistance or impart synergistic effects on MM therapy. For example, the triplet combination of pomalidomide (POM), bortezomib (BTZ), and low-dose dexamethasone (DEX) has demonstrated clinical benefits in R/RMM after previous therapy with lenalidomide (LEN) and a PI.[10,11] The synergistic antitumor effects between doublet regimens of POM in combination with BTZ or DEX have been reported in preclinical models.[12,13] Similarly, MEZI combination regimens are being investigated preclinically[5,14-16] and in patients with R/RMM. Although MEZI has demonstrated superior preclinical activity compared with similar agents, a detailed analysis of its mechanisms in triplet combinations are lacking.

Similar to IMiD agents such as LEN and POM, the molecular mediator of MEZI is CRBN, a substrate receptor of the CUL4A-E3 ubiquitin ligase complex ($CRL4^{CRBN}$).[4,17-19] Binding of these compounds to CRBN elicits recruitment of neomorphic substrates, including the essential hematologic lineage MM transcription factors Aiolos and Ikaros, to $CRL4^{CRBN}$ with their subsequent poly-ubiquitination and proteasome-dependent degradation.[4,20-22] Although LEN, POM, and MEZI have similar mechanisms, MEZI has a higher binding affinity and specificity for CRBN, resulting in more efficient recruitment and rapid degradation of neosubstrates.[4,5] These differences result in MEZI's enhanced potency, broader antitumor activity, and potentially reduced resistance, which may translate to better clinical outcomes for patients with MM. In addition, recent structural studies of POM and MEZI bound to CRBN show distinct induced stoichiometry of open and closed loop conformations, potentially explaining variations in substrate recruitment efficiencies, kinetics, and potencies.[22]

BTZ, a reversible PI, affects multiple signaling cascades and other homeostatic processes leading to MM cell death.[23,24] Despite potential antagonism on both cell autonomous and immunomodulatory mechanisms, clinical evidence suggests complementarity between PIs, IMiD/CELMoD molecules, and DEX.[10,11,25-27] The POM/BTZ/DEX triplet regimen's success may be attributed to temporal differences in the scheduled administration and nonoverlapping pharmacokinetics of each agent during therapy.[11,28,29]

This study highlights the characteristics of MEZI as a next-generation CELMoD and outlines the potential triplet MOA when combined with BTZ and DEX, supporting its therapeutic rationale in the clinical setting.

Materials and methods

Reagents

POM and MEZI were provided by Bristol Myers Squibb (San Diego, CA). BTZ and DEX were obtained from Selleck Chemical (Houston, TX). Stock solutions were prepared in dimethyl sulfoxide (DMSO; Thermo Fisher Scientific, Waltham, VA).

Cell lines

Human MM cell lines were obtained from American Type Culture Collection (Manassas, VA). Cells were maintained in RPMI 1640 medium (Corning Cellgro; Manassas, VA) with 10% heat inactivated fetal bovine serum (Thermo Fisher Scientific), 1× glutamate, 1× penicillin/streptomycin, and 1× pyruvate (ThermoFisher). Cell lines were routinely tested for mycoplasma (Lonza; Bend, OR) and authenticated by short tandem repeat fingerprinting (AmpFlSTR, ThermoFisher) according to the manufacturer's protocol. LEN-resistant H929 cells (H929-1054) were generated and maintained as previously described.[13]

Additional materials and methods details can be found in the supplemental Materials.

Results

Cytotoxic effects of MEZI compared with POM in combination with BTZ and DEX

Initial studies of MEZI showed superior anti-MM activity when compared with POM,[4] with MEZI being 50- to 100-fold more potent (MEZI 50% inhibitory concentration [IC_{50}] of ~ 0.07nM-0.08nM vs POM IC_{50} of ~ 5nM-7nM) in H929 and MM1.S cells (supplemental Figure 1A). MEZI also demonstrated a dose- and time-dependent inhibition of cell growth and increased apoptosis at doses 100-fold lower than POM (Figure 1A).

To compare MEZI and POM in combination with BTZ with/without (w/wo) DEX, we evaluated 2 BTZ exposure methods: high-dose pulse (1 hour followed by drug washout, reflective of clinical pharmacokinetic exposure[30]) and continuous low dose. We observed an ~25-fold decrease in sensitivity (pulse IC_{50} of ~20nM-50nM vs continuous IC_{50} of ~0.8nM-2nM) in H929 and MM1.S cells (supplemental Figure 1B). Given its closer alignment with clinical settings, the BTZ-pulse method was chosen to further explore combination studies.

Titrating combinations of either POM or MEZI with BTZ, showed a strong anti-MM effect as shown by the inhibition of proliferation (Figure 1B) and concomitant annexin V–positive staining (Figure 1C) in MM1.S or H929 cells over time, with similar or pronounced effects with MEZI at a 100-fold lower dose range. Synergistic effects of the combination of either MEZI or POM in combination with BTZ was determined by excess over Bliss (supplemental Figure 2A-D). Longitudinal relative cell growth of H929 or MM1.S treated with MEZI alone, or in combination with BTZ w/wo DEX, showed diminished cell growth compared with vehicle control or POM, for which the order of efficacy followed triplets > doublets > singlets (Figure 1D). The inhibitory effects on proliferation of either single agent or combinations on cell growth inversely correlated with the temporal increase in relative apoptosis (Figure 1E). Additional MM cell lines with a range of sensitivities to IMiD agents were also tested, including AMO1, JJN3, LP1, and RPMI8226, and the LEN-resistant H929LR (H929-1054) cell line, in which similar patterns of antiproliferative effects were observed with the indicated treatments (supplemental Figure 3A-E). Together, MEZI was more effective than POM in all configurations, even at a 20- to 100-fold lower concentration.

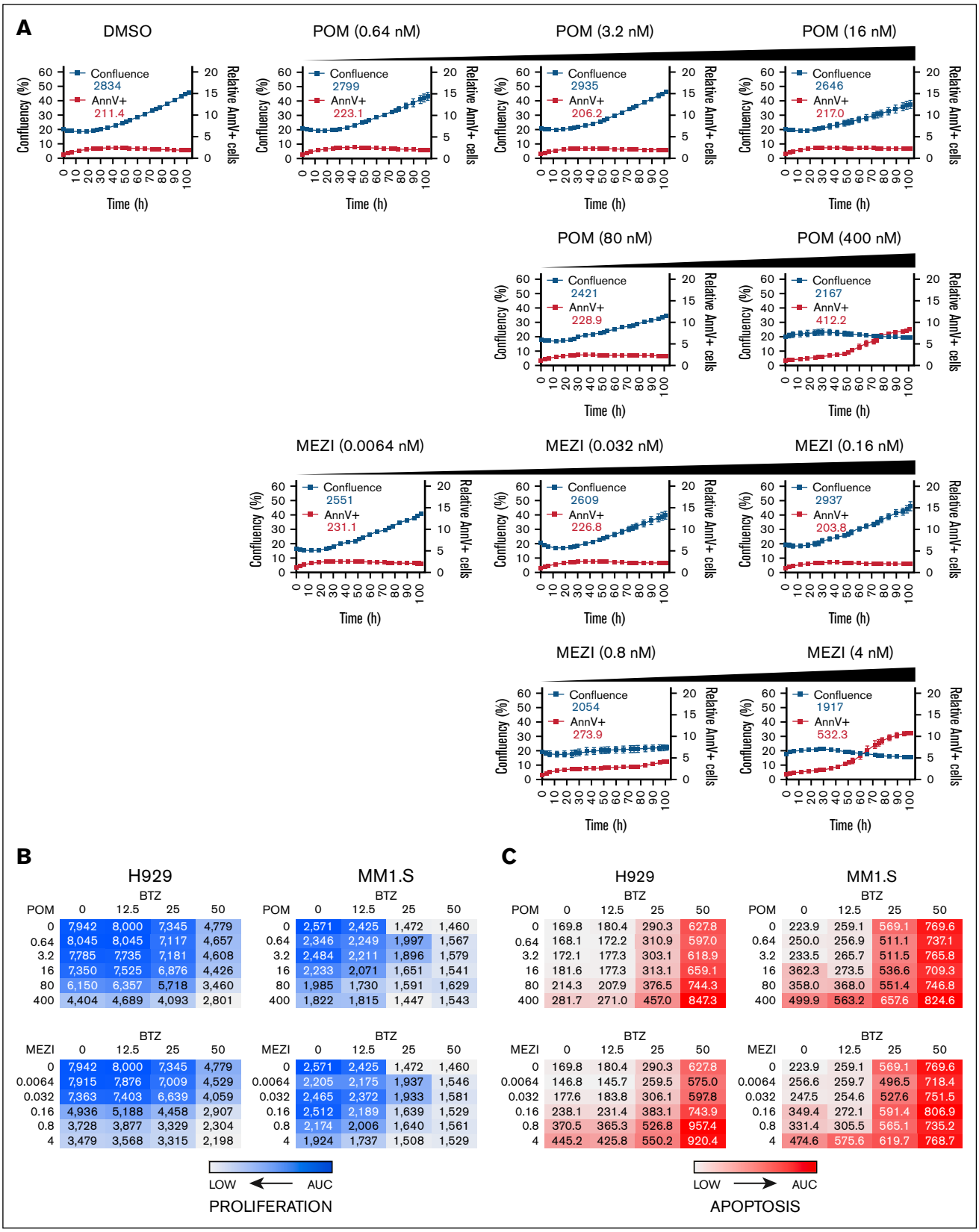

Figure 1. Antiproliferative and proapoptotic effects of POM or MEZI in combination with BTZ and DEX in MM cell lines. (A) Longitudinal cell growth (0-105 hours) assessed by phase-contrast confluence (blue line and blue area under the curve [AUC] value) or relative apoptotic cells via annexin-V positive (AnnV+) staining (red line; normalized to 0 hours, and red AUC value) of MM1.S cells after treatment with either DMSO, POM (0.64nM-400nM) or MEZI (0.0064nM-4nM). (B) AUC heat map showing

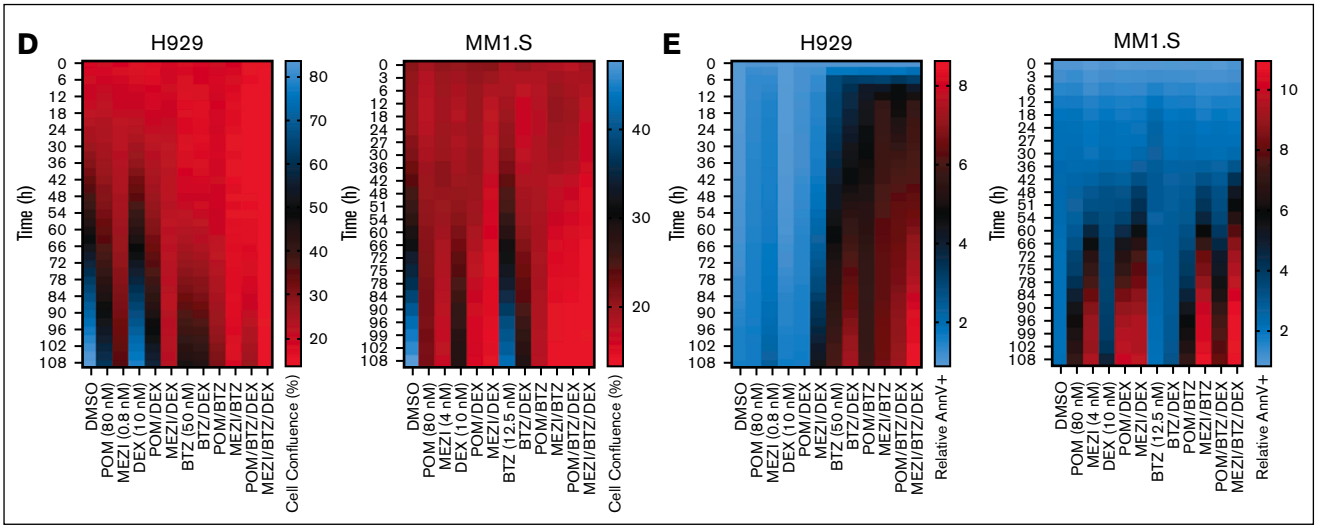

Figure 1 (continued) relative antiproliferative effects of either POM (0.64nM-400nM) or MEZI (0.0064nM-4nM) in combination with BTZ-pulse (0nM-50nM) from longitudinal phase-contrast confluency in H929 and MM1.S cells. (C) AUC heat map of showing relative proapoptotic effects of matched data described and collected in panel B for H929 and MM1.S cells. (D) Percent cell growth (0-105 hours) assessed by phase-contrast confluence of H929 or MM1.S cells after treatment with DMSO, POM (80nM), MEZI (0.4nM or 4nM), BTZ-pulse (12.5nM or 50nM), and DEX (10nM) as single agents, or doublet or triplet combinations. (E) Relative apoptotic cell death (normalized to time 0) determined by AnnV+ staining of matched data described and collected in panel D. All data shown as representatives of replicate experiments.

Faster substrate degradation of substrates by MEZI than POM in combination with BTZ w/wo DEX in MM cells

We previously described the relationship of the rate of endogenous proteasomal-dependent substrate degradation between LEN and POM.[20] However, the potential antagonistic effects of BTZ on the rate of IMiD- or CELMoD-induced endogenous substrate degradation have not been studied. To compare the rate of substrate depletion by MEZI and POM as single agents, and in combination, we first confirmed the activity of the BTZ-pulse method. BTZ preferentially inhibits chymotrypsin-like (CT-L) activity, with lesser inhibition of caspase-like (C-L) and minimal inhibition of trypsin-like.[31] CT-L activity decreased by ~90% at 1 hour after BTZ washout, recovering to >80% at 24 hours, both alone and in combination with POM, MEZI, and/or DEX (supplemental Figure 4A). C-L activity was inhibited by ~30% to 40% and recovered to ~80% at 24 hours (supplemental Figure 4B), whereas trypsin-like activity showed minimal inhibition at 1 hour after BTZ-pulse washout (supplemental Figure 4C).

The relative kinetic depletion of Aiolos/Ikaros by MEZI was compared with POM using approximate clinical concentrations with BTZ w/wo DEX. Intracellular flow cytometry in H929 and MM1.S cells showed that MEZI or POM alone reduced Aiolos (Figure 2A,C) and Ikaros (Figure 2B,D) levels by ~60% and ~30%, respectively, within 0.5 to 1 hour, with MEZI reaching 80% to 95% depletion at 6 hours. MEZI alone and with DEX reached 50% depletion (T_{50}) for Aiolos/Ikaros at 0.8 to 0.9 and 1.1 to 1.4 hours, respectively, whereas POM w/wo DEX was slower, with T_{50} of 2.5 to 5.2, to 4.7 to >6 hours (supplemental Figure 4D-E). MEZI, at 100-fold lower dose, was ~3.1- to 5.8-times faster than POM in depleting endogenous Aiolos/Ikaros, in the absence of BTZ. This correlates with MEZI's enhanced antiproliferative and proapoptotic effects, attributed, in part, to its unique CRBN-binding characteristics.[22] BTZ alone or with DEX did not affect Aiolos/Ikaros levels early on, but BTZ with POM or MEZI delayed depletion by 3 to 6 hours (Figure 2A-D; supplemental Figure 4D-E). Immunoblotting and semiquantitative assessment of Aiolos/Ikaros confirmed the relative effect of POM or MEZI in the absence or presence of BTZ (Figure 2E; supplemental Figure 4F-G). At 6 hours, CT-L and C-L activities were inhibited by ~60% and ~35%, respectively, with POM-induced substrate depletion more affected by BTZ than MEZI (~20% vs ~60%, respectively; Figure 2F), highlighting MEZI's superior efficiency in overcoming proteasome inhibition. RNA sequencing and reverse transcription polymerase chain reaction analysis showed little to no change in relative Aiolos/Ikaros transcript levels (data not shown), confirming that protein reduction was not due to transcriptional downregulation.

MEZI, in combination with BTZ, induces a dysregulation of the cell cycle

Previous studies have shown that IMiDs and CELMoDs induce cell cycle arrest, particularly in G1.[32-34] To further investigate this, we assessed the effects of MEZI or POM, alone or in combination with BTZ w/wo DEX in H929 cells. At 72 hours, both POM (~63%-70%) and MEZI (~79%-83%) alone caused a sustained G0/G1 arrest compared with DMSO control (~52%), with minor sub-G1 accumulation (6%-8%; supplemental Figure 5A-B). The addition of DEX slightly enhanced G0/G1 arrest, consistent with previous findings.[12,13,33] BTZ alone induced an increase in both G0/G1 (~65% vs ~48% DMSO) and G2/M (~24% vs ~18% DMSO) at 24 to 48 hours, and a slightly delayed but sustained accumulation of sub-G1 (~19%-42% vs 2% DMSO) at 48 to 72 hours (supplemental Figure 5A-B). POM/BTZ and POM/BTZ/DEX combinations increased in G0/G1 (~65% and 59% at 24 hours) compared with single treatments, in which the sub-G1 fraction increased over time. MEZI/BTZ and MEZI/BTZ/DEX increased the G2/M fraction at 24 hours compared with BTZ alone (~30% and

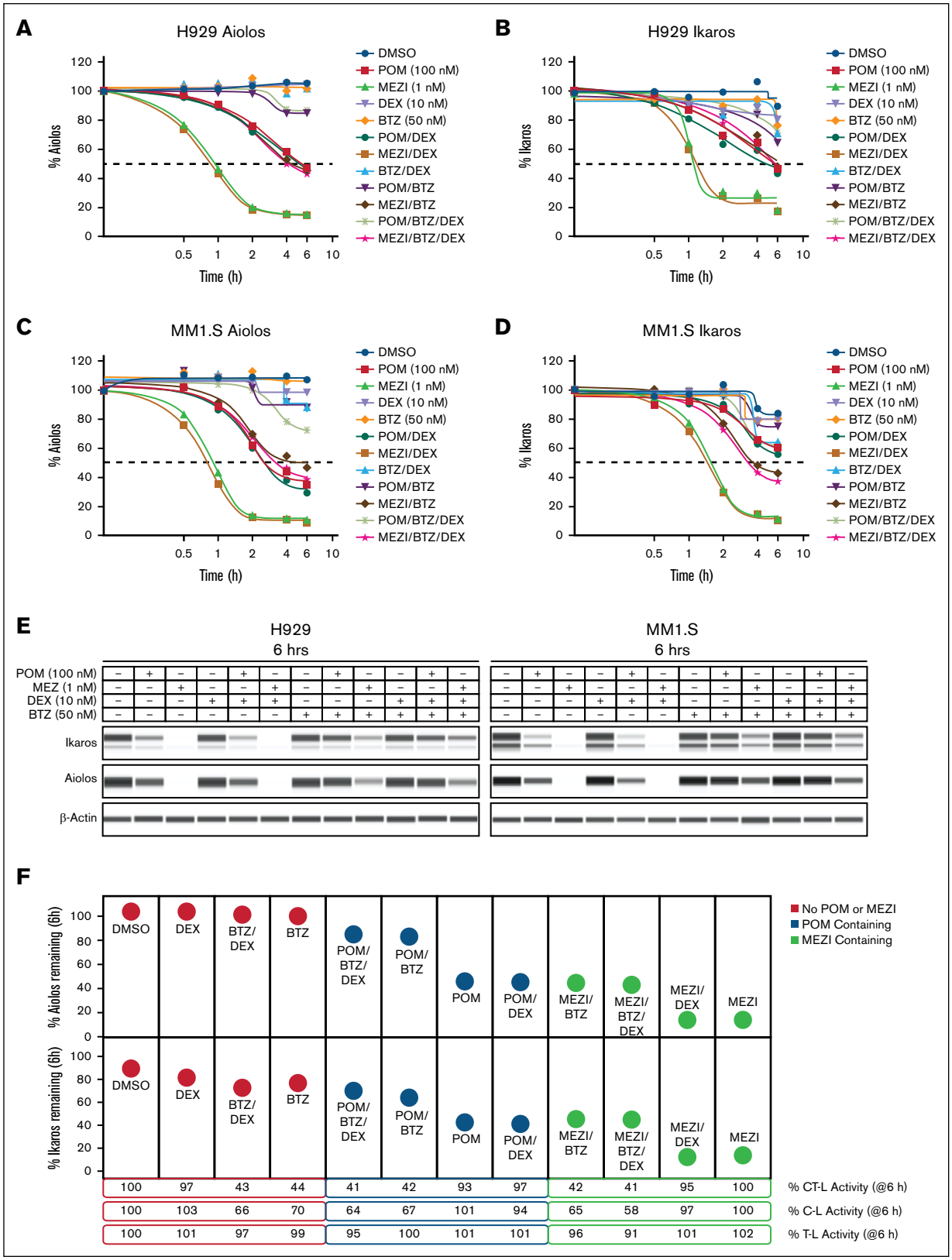

Figure 2. Evaluation of POM or MEZI drug mechanism as single agents and in combination with BTZ and DEX on MM cells. Intracellular flow cytometric analysis of the relative abundance (% normalized to DMSO control at 100%) in H929 for Aiolos (A) or Ikaros (B), or MM1.S for Aiolos (C) or Ikaros (D) after treatment with either single agents POM (100nM), MEZI (1nM), BTZ-pulse (50nM), or DEX (10nM), or in doublet or triplet combinations, at 0, 0.5, 1, 2, 4, and 6 hours. All data shown as representatives of

~32% vs ~24%; supplemental Figure 5A). Time-dependent cell cycle effects were confirmed by averaging changes in cell cycle distribution in H929 and MM1.S cells (supplemental Figure 5C). All treatments, except BTZ, and MEZI/BTZ combinations, increased G0/G1 fractions at 24 hours, indicating G0/G1 arrest. Beyond 24 hours, G0/G1 arrest was sustained in all treatments except those containing BTZ, which decreased between 48 and 72 hours, corresponding to an increase in sub-G1.

Using EdU (5-ethynyl-2'-deoxyuridine) incorporation and DNA staining, we further investigated the effects of single agents and combinations on the cell cycle at additional time points (12, 16, 24, and 48 hours) in H929 and MM1.S cells. At 12 and 16 hours, all treatments, except DEX, increased the G0/G1 fraction, in which MEZI and BTZ were ~76% and ~72% compared with control (~59%) at 16 hours (Figure 3A; supplemental Figure 6A-B). BTZ-containing treatments resulted in an increase in the G2/M fraction, as a single agent and in combination with either POM or MEZI, which was further increased at all time points. At 16 hours, the MEZI/BTZ/DEX combination resulted in a nearly nonexistent S-phase, in which all cells were in either G0/G1 or G2/M compared with BTZ alone or POM/BTZ/DEX. EdU incorporation confirmed that the addition of POM or MEZI increases the G2/M fraction compared with BTZ alone, albeit incrementally more with MEZI.

To complement our observations on the effects of MEZI in combination with BTZ on cell cycle, we used a fluorescent ubiquitination-based cell cycle indicator (FUCCI) to monitor relative cell cycle distribution in H929 cells. In DMSO-treated cells, the relative distribution of highly viable cells (>95%) was proportionally identified as G1, G1/S, or G2/M based upon their FUCCI markers at time 0. The normal oscillation pattern of this distribution was observed over the doubling time (70-78 hours) of H929 cells (Figure 3B; DMSO). At time 0, ~50% of H929-FUCCI were in G1 + G1/S (green and red), and ~50% were in G2/M (Figure 3B; blue). The distribution shifted to ~55% in G1 + G1/S at 24 hours, decreased to ~45% at 60 hours, and reverted to ~50% at >72 hours, consistent with the oscillatory pattern seen in other cancer cell types in vitro,[35] although slower due to the longer doubling time of MM cells. Both single-agent POM and MEZI confirmed a G0/G1 arrest, with the G1 + G1/S distribution increasing to ~65% in the first 24 hours, which was then sustained over the duration for POM. MEZI treatment showed an eventual decline in the G1 + G1/S with correlating increases in G2/M. Single-agent BTZ caused a gradual and sustained increase in G2/M population indicating G2/M arrest. Combinations of BTZ with POM, w/wo DEX, showed cell cycle distributions combining patterns observed with the single agents, with G1 + G1/S and G2/M signals both around ~50%, slightly favoring G2/M toward the end. Notably, MEZI combined with BTZ, especially with DEX, resulted in a pronounced increase in the G2/M population, reaching ~90% by the end of the observation period. Relative confluency assessments (Figure 3B; yellow dots) indicated similar confluency patterns between POM/BTZ/DEX and MEZI/BTZ/DEX but divergent cell cycle distributions.

Additionally, H929 cells treated with either POM or MEZI containing triplets for 24 hours were stained for histone H3-pSer10, a marker associated with different chromatin condensation states and stages of the cell cycle, including accumulation during G2/M.[36] Immunofluorescent microscopic images comparing the H3-pSer10 staining pattern between vehicle control, POM/BTZ/DEX, or MEZI/BTZ/DEX, identified cells within G1, G2, or M phases, in which we observed increases in total H3-pSer10 in the MEZI/BTZ/DEX treatment, indicative of an increase in G2/M (supplemental Figure 6C). Relative quantitation of the H3-pSer10 signal indicated a significant increase in the MEZI/BTZ/DEX-treated sample (supplemental Figure 6D).

Our observations that MEZI combined with BTZ disrupted the cell cycle led us to explore potential mechanisms by differentiating the relative effects of triplet combinations on gene expression by RNA sequencing. Single-agent POM, MEZI, DEX, or BTZ, and the triplet combinations showed the differentially expressed genes (DEGs) resulting from all treatments, in which the triplets were dominated by changes induced by POM or MEZI (Figure 4A). Accordingly, gene set enrichment analysis of HALLMARK pathways comparing the different treatments showed that most pathways are changed in a similar direction in the triplet combinations compared with either POM or MEZI (Figure 4B). Therefore, we directly compared the DEG between MEZI/BTZ/DEX vs POM/BTZ/DEX, and subsequent gene set enrichment analysis from non-HALLMARK pathways. We observed consistent differences in the negative enrichment of several annotated cell cycle–associated pathways, including the regulation of the mitotic cell cycle and the role of GTSE1 in G2/M progression after G2 checkpoint (Figure 4C). Volcano plot analysis of the DEG identified in the latter (and most significant) pathway revealed downregulation of genes primarily associated with proteasomal subunits (ie, *PSMA*, *PSMB*, *PSMC*, and *PSMD* genes) in the MEZI/BTZ/DEX treatment compared with POM/BTZ/DEX (Figure 4D). To see whether the changes in proteasomal subunit gene expression were the result of direct transcriptional regulation by IMiD/CELMoD substrates, we performed chromatin immunoprecipitation with sequencing analysis of Ikaros, with and without MEZI single-agent treatment. As a result, we found that many of these genes have a corresponding Ikaros peak near the promoter/transcription start site, that is displaced upon treatment with MEZI (Figure 4E). Additionally, we observed differences in genes associated with the mitotic cell cycle phase transition, including Aurora kinases, cyclins, cyclin-dependent kinases, cyclin-dependent kinase inhibitors, and checkpoint transcripts, that also corresponded to Ikaros binding near their respective promoter/transcription start site (supplemental Figure 7A).

Figure 2 (continued) replicate experiments (minimum n = 3). (E) Immunoblot staining of Aiolos/Ikaros in H929 or MM1.S cells after 6 hours treatment with either DMSO; single-agent POM (100nM), MEZI (1nM), BTZ-pulse (50nM), and DEX (10nM); or in doublet or triplet combinations. (F) Comparison of the relative levels of Aiolos or Ikaros remaining (%), and relative proteasomal CT-L, T-L, and C-L activity after 6-hour treatment with either DMSO; single-agent POM (100nM), MEZI (1nM), BTZ-pulse (50nM), and DEX (10nM); or in doublet or triplet combinations in H929 cells. Non-POM– or non-MEZI–containing treatments are shown in red, POM-containing treatments in blue, and MEZI-containing treatments in green. All data shown as representatives of replicate experiments. T-L, trypsin-like.

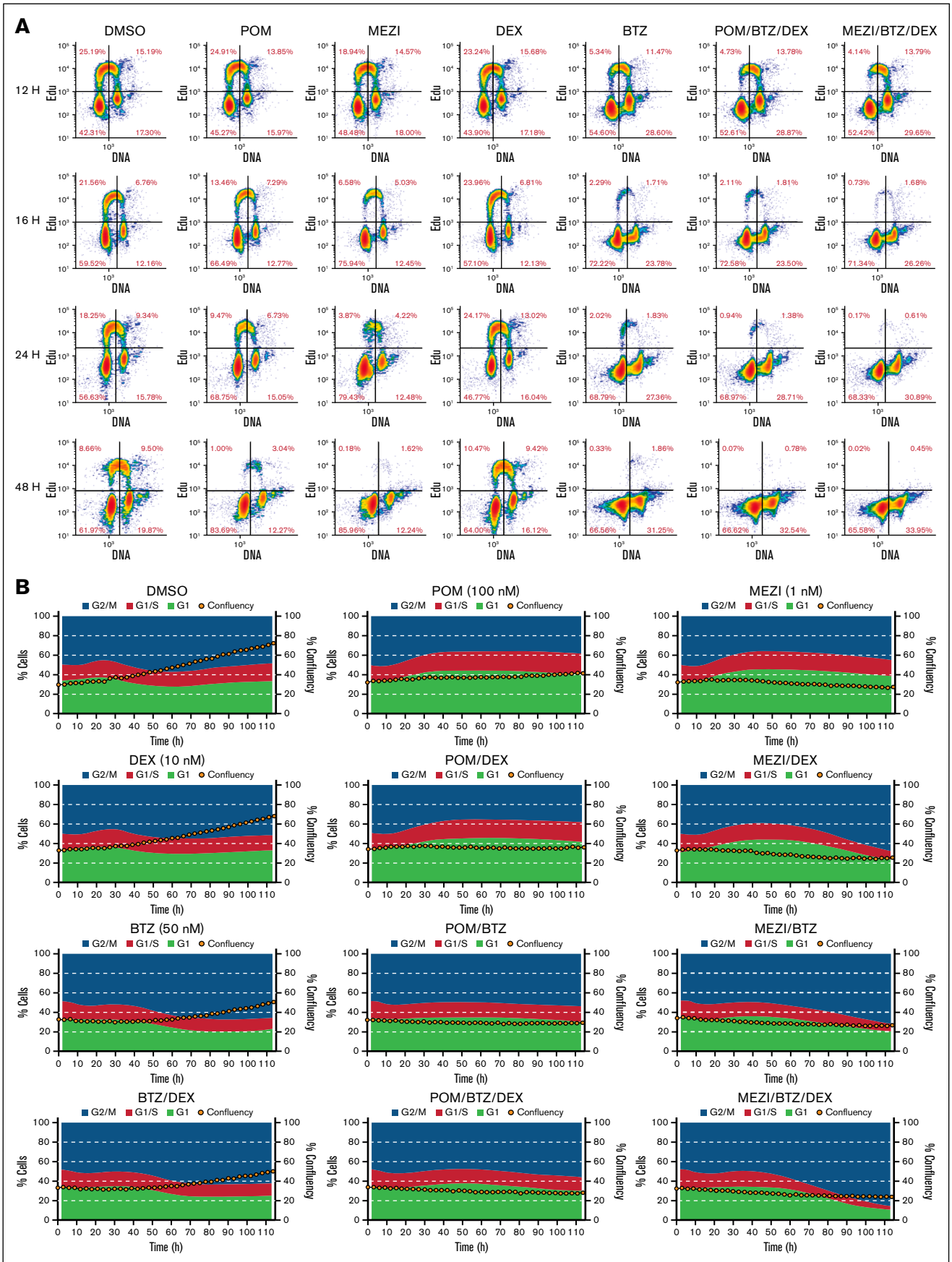
A
DMSO
POM
MEZI
DEX
BTZ
POM/BTZ/DEX
MEZI/BTZ/DEX
12 H
16 H
24 H
48 H
Edu
DNA
25.19% 15.19% 42.31% 17.30%
24.91% 13.85% 45.27% 15.97%
18.94% 14.57% 48.48% 18.00%
23.24% 15.68% 43.90% 17.18%
5.34% 11.47% 54.60% 28.60%
4.73% 13.78% 52.61% 28.87%
4.14% 13.79% 52.42% 29.65%
21.56% 6.76% 59.52% 12.16%
13.46% 7.29% 66.49% 12.77%
6.58% 5.03% 75.94% 12.45%
23.96% 6.81% 57.10% 12.13%
2.29% 1.71% 72.22% 23.78%
2.11% 1.81% 72.58% 23.50%
0.73% 1.68% 71.34% 26.26%
18.25% 9.34% 56.63% 15.78%
9.47% 6.73% 68.75% 15.05%
3.87% 4.22% 79.43% 12.48%
24.17% 13.02% 46.77% 16.04%
2.02% 1.83% 68.79% 27.36%
0.94% 1.38% 68.97% 28.71%
0.17% 0.61% 68.33% 30.89%
8.66% 9.50% 61.97% 19.87%
1.00% 3.04% 83.69% 12.27%
0.18% 1.62% 85.96% 12.24%
10.47% 9.42% 64.00% 16.12%
0.33% 1.86% 66.56% 31.25%
0.07% 0.78% 66.62% 32.54%
0.02% 0.45% 65.58% 33.95%
B
DMSO
POM (100 nM)
MEZI (1 nM)
DEX (10 nM)
POM/DEX
MEZI/DEX
BTZ (50 nM)
POM/BTZ
MEZI/BTZ
BTZ/DEX
POM/BTZ/DEX
MEZI/BTZ/DEX
G2/M
G1/S
G1
Confluency
% Cells
% Confluency
Time (h)

Figure 3.

MEZI triplet treatment leads to rapid, sustained regression and survival of a LEN-resistant xenograft MM tumor model

A LEN-resistant (H929-1054)[13] xenograft model was established to evaluate antitumor and survival efficacy of doublet and triplet combinations of POM or MEZI. POM/DEX treatment moderately delayed tumor growth, followed by a more significant delay with the BTZ/DEX and MEZI/DEX cohorts (Figure 5A-B). POM/BTZ/DEX showed a marked improvement controlling tumor growth compared with POM/BTZ. The MEZI/BTZ doublet affected the tumor growth rate and subsequent reduction similarly to POM/BTZ/DEX until day 41, with a significant improvement of tumor growth control with MEZI/BTZ beyond day 41. The MEZI/BTZ/DEX triplet saw a fast regression of tumor volume, within 5 days, followed by continuous and sustained reduction to a near complete loss of palpable tumor detection on average, by day 41. Plots of individual tumor growth response to vehicle, POM/BTZ/DEX, or MEZI/BTZ/DEX (Figure 5C), indicated that 8 of 10 mice relapsed on POM/BTZ/DEX and nearly all the mice in the MEZI/BTZ/DEX cohort had minimal measurable tumors. Survival analysis showed that 100% of mice in the MEZI/BTZ/DEX cohort remained alive over the course of the observation period, including 14 days after dosing (Figure 5D). Ranked efficacy shows that the MEZI/BTZ/DEX treatment was significantly superior (median overall survival [mOS] not reached), followed by MEZI/BTZ (mOS of 71 days), POM/BTZ/DEX (mOS of 66 days), and POM/BTZ (mOS of 52 days; Figure 5D-E).

MEZI/BTZ/DEX reduces bone marrow disease burden and increases mOS in a humanized CRBN syngeneic MM mouse model

To further evaluate the effects of triplet regimens in vivo, we used a murine cell line (MM5080^{WT}) derived from a transgenic, genetically engineered mouse model of MM.[37] In order to use the MM5080^{WT} cell line so that it would be sensitive to the cytotoxic effects of either POM or MEZI, we used a CRISPR-based editing approach to modify wild-type murine *CRBN* to introduce a single-codon change, I391V (MM5080^{CRBNI391V}) that has been shown to be sufficient for IMiD/CELMoD binding and subsequent pharmacodynamic activity in mouse models.[38] After single-cell clonal selection and validation of the genetic alteration, we tested the ability of MEZI to induce degradation of Aiolos/Ikaros in vitro (supplemental Figure 8A-C). Compared with MM5080^{WT}, MEZI efficiently induced the degradation of murine Aiolos/Ikaros in a dose- and time-dependent manner in MM5080^{CRBNI391V}.

Subsequently, a syngeneic MM model was generated by engrafting the MM5080^{CRBNI391V} cell line in C57BL6^{CRBNI391V} mice to generate an immunocompetent in vivo MM model to evaluate antitumor, immune, and survival effects of the POM/BTZ/DEX and MEZI/BTZ/DEX triplet regimens. Compared with vehicle control (mOS of 26.5 days), the POM/BTZ/DEX triplet did not show any significant improvement in survival (mOS of 28 days; Figure 6A). However, the MEZI/BTZ/DEX therapy showed a significant improvement in survival (mOS of 38 days). During disease and treatment, a small number of mice were euthanized from each cohort at day 22 (n = 5 each) to evaluate measurable bone marrow involved disease (green fluorescent protein–positive [GFP$^+$] MM5080^{CRBNI391V} plasma cells [PCs]) and non-PC immune populations from flushed bone marrow. Relative total percentages of GFP$^+$ PC (PC^{GFP+}) MM cells constituted a very small fraction (<10% except for 1 control sample of ~20%) of total cells evaluated, with a nonstatistically significant trend of reduced levels of MM cells with either the POM/BTZ/DEX or MEZI/BTZ/DEX treatments compared with the control group (Figure 6B). Analysis of select immune populations indicated a significant decrease in total CD19$^+$ cells (Figure 6C).

Lastly, we were able to perform multiplex immunofluorescence staining of formalin-fixed and paraffin-embedded preserved femurs for PC^{GFP+} and CD8$^+$ cells (Figure 6K). We confirmed the presence of engrafted PC^{GFP+} infiltration within the bone marrow in which it displayed a diffuse spatiality with relatively little CD8$^+$ cells within the tumor associated area in control mice. By comparison, we observed a trending reduction of PC^{GFP+}, and increased tumor area infiltration of CD8$^+$ cells, with both the POM/BTZ/DEX and MEZI/BTZ/DEX treatments, with the biggest observable difference being in the MEZI/BTZ/DEX combination, suggesting a treatment-induced immune response facilitated by CD8$^+$ clearance of PC^{GFP+} cells. In addition to more enhanced clearance of PC^{GFP+}, we observed an increase in double-positive CD8$^+$/granzyme B–positive cytotoxic T-cell infiltration (Figure 6E-F). These observations support the survival advantage associated with the MEZI/BTZ/DEX treatment in this syngeneic mouse model of MM.

Discussion

This work provides new insights on the mechanistic interplay between proteasome inhibition and CRBN modulating compounds, particularly their combined effect on disrupting multiple phases of the cell cycle. Theoretically, PIs could be antagonistic to IMiD or CELMoD agents by blocking the proteolytic degradation of Aiolos/Ikaros.[27,39] In preclinical studies, pulsing of BTZ showed maximal inhibition of the β5-associated CT-L activity within the first hour, with rapid recovery over 24 hours, mirroring the clinical pharmacokinetics after IV administration.[24,29,30,40] When combined with MEZI, BTZ attenuated the initial rate of depletion of endogenous Aiolos/Ikaros but not the final extent of depth (data not shown). These observations have important clinical implications. First, rapid degradation of substrates is a hallmark of potency and has been used as a differentiating characteristic among these compounds.[20] The relative delay of substrate degradation, due to proteasome inhibition, could be expected to lessen the potency of the compounds and could hypothetically abrogate the superior antiproliferative and proapoptotic effects of CELMoD over IMiD agents. However, this is not the case, because multiple studies

Figure 3. Cell cycle analysis of POM or MEZI in combination with BTZ and DEX in MM cells. (A) Treatment of H929 cells with either DMSO control; single-agent POM (100nM), MEZI (1nM), BTZ-pulse (50nM), and DEX (10nM); or in triplet combinations for 12, 16, 24, or 48 hours followed by cell cycle analysis using EdU$^+$ incorporation. (B) Longitudinal (0-110 hours) imaging analysis of stably transduced H929-FUCCI cells for cell cycle distribution (left y-axis) in either G1 (green), G1/S transition (red), or G2/M (blue) overlaid on the percentage (%) confluency (orange dots, right y-axis), after treatment with either DMSO; single-agent POM (100nM), MEZI (1nM), BTZ-pulse (50nM), and DEX (10nM); or in combination. All data shown as representatives of replicate experiments.

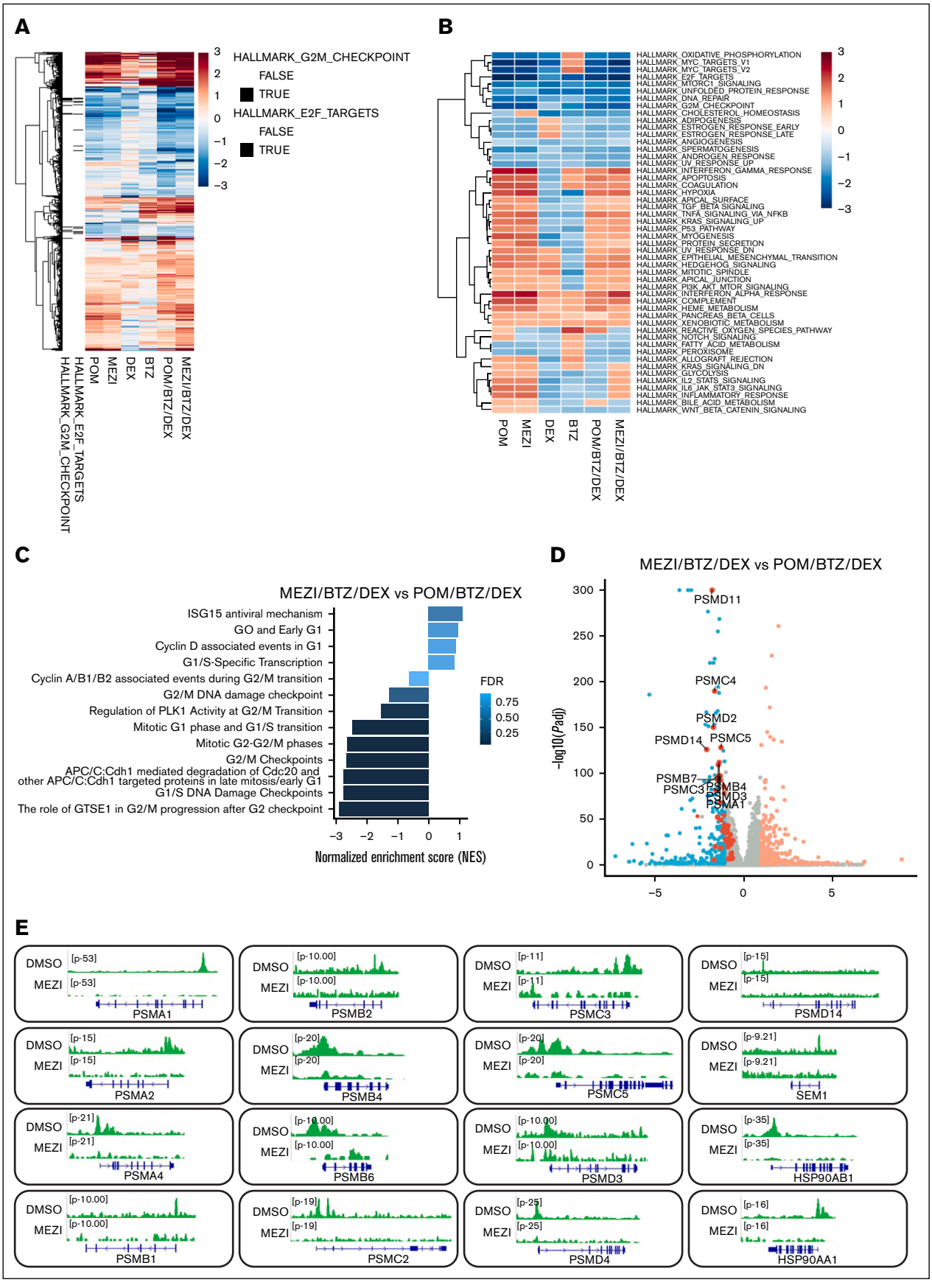
A
HALLMARK_G2M_CHECKPOINT
HALLMARK_E2F_TARGETS
POM
MEZI
DEX
BTZ
POM/BTZ/DEX
MEZI/BTZ/DEX
HALLMARK_G2M_CHECKPOINT
FALSE
TRUE
HALLMARK_E2F_TARGETS
FALSE
TRUE
B
HALLMARK_OXIDATIVE_PHOSPHORYLATION
HALLMARK_MYC_TARGETS_V1
HALLMARK_MYC_TARGETS_V2
HALLMARK_E2F_TARGETS
HALLMARK_MTORC1_SIGNALING
HALLMARK_UNFOLDED_PROTEIN_RESPONSE
HALLMARK_DNA_REPAIR
HALLMARK_G2M_CHECKPOINT
HALLMARK_CHOLESTEROL_HOMEOSTASIS
HALLMARK_ADIPOGENESIS
HALLMARK_ESTROGEN_RESPONSE_EARLY
HALLMARK_ESTROGEN_RESPONSE_LATE
HALLMARK_ANGIOGENESIS
HALLMARK_SPERMATOGENESIS
HALLMARK_ANDROGEN_RESPONSE
HALLMARK_UV_RESPONSE_UP
HALLMARK_INTERFERON_GAMMA_RESPONSE
HALLMARK_APOPTOSIS
HALLMARK_COAGULATION
HALLMARK_HYPOXIA
HALLMARK_APICAL_SURFACE
HALLMARK_TGF_BETA_SIGNALING
HALLMARK_TNFA_SIGNALING_VIA_NFKB
HALLMARK_KRAS_SIGNALING_UP
HALLMARK_P53_PATHWAY
HALLMARK_MYOGENESIS
HALLMARK_PROTEIN_SECRETION
HALLMARK_UV_RESPONSE_DN
HALLMARK_EPITHELIAL_MESENCHYMAL_TRANSITION
HALLMARK_HEDGEHOG_SIGNALING
HALLMARK_MITOTIC_SPINDLE
HALLMARK_APICAL_JUNCTION
HALLMARK_PI3K_AKT_MTOR_SIGNALING
HALLMARK_INTERFERON_ALPHA_RESPONSE
HALLMARK_COMPLEMENT
HALLMARK_HEME_METABOLISM
HALLMARK_PANCREAS_BETA_CELLS
HALLMARK_XENOBIOTIC_METABOLISM
HALLMARK_REACTIVE_OXYGEN_SPECIES_PATHWAY
HALLMARK_NOTCH_SIGNALING
HALLMARK_FATTY_ACID_METABOLISM
HALLMARK_PEROXISOME
HALLMARK_ALLOGRAFT_REJECTION
HALLMARK_KRAS_SIGNALING_DN
HALLMARK_GLYCOLYSIS
HALLMARK_IL2_STAT5_SIGNALING
HALLMARK_IL6_JAK_STAT3_SIGNALING
HALLMARK_INFLAMMATORY_RESPONSE
HALLMARK_BILE_ACID_METABOLISM
HALLMARK_WNT_BETA_CATENIN_SIGNALING
POM
MEZI
DEX
BTZ
POM/BTZ/DEX
MEZI/BTZ/DEX
C
MEZI/BTZ/DEX vs POM/BTZ/DEX
ISG15 antiviral mechanism
GO and Early G1
Cyclin D associated events in G1
G1/S-Specific Transcription
Cyclin A/B1/B2 associated events during G2/M transition
G2/M DNA damage checkpoint
Regulation of PLK1 Activity at G2/M Transition
Mitotic G1 phase and G1/S transition
Mitotic G2-G2/M phases
G2/M Checkpoints
APC/C:Cdh1 mediated degradation of Cdc20 and other APC/C:Cdh1 targeted proteins in late mitosis/early G1
G1/S DNA Damage Checkpoints
The role of GTSE1 in G2/M progression after G2 checkpoint
FDR
0.75
0.50
0.25
Normalized enrichment score (NES)
D
MEZI/BTZ/DEX vs POM/BTZ/DEX
−log10(Padj)
PSMD11
PSMC4
PSMD2
PSMD14
PSMC5
PSMB7
PSMC3
PSMB4
PSMD3
PSMA1
E
DMSO
MEZI
PSMA1
PSMB2
PSMC3
PSMD14
PSMA2
PSMB4
PSMC5
SEM1
PSMA4
PSMB6
PSMD3
HSP90AB1
PSMB1
PSMC2
PSMD4
HSP90AA1

Figure 4.

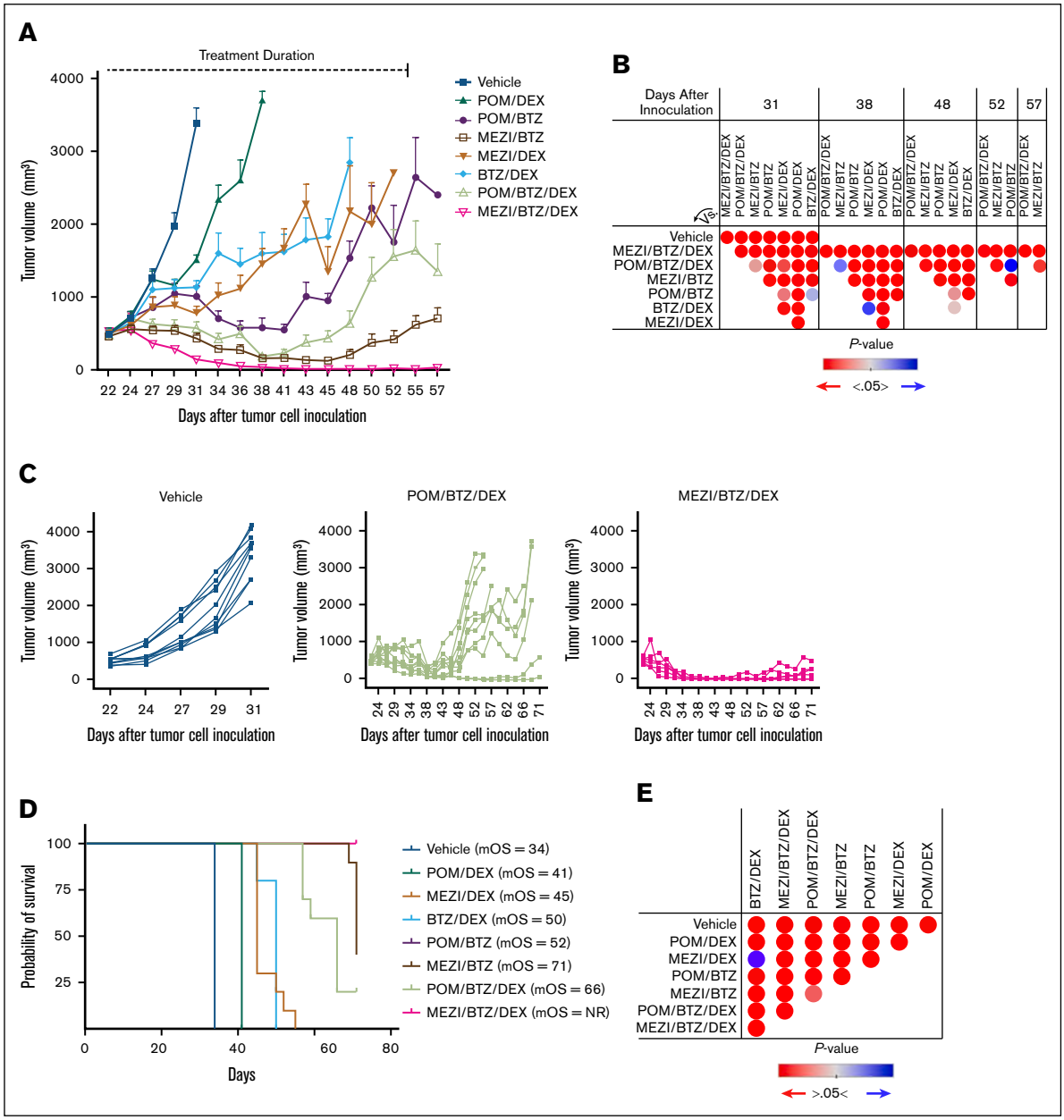

Figure 5. Efficacy of doublet or triplet combinations in a LEN-resistant xenograft model. LEN-resistant H929 (H929-1054) cells were subcutaneously xenografted into NSG (NOD-SCID gamma) mice and tumor volume was allowed to reach 500 mm^3 before treatment. Overall, 8 cohorts (n = 10 mice per cohort) were dosed with either vehicle, or POM/DEX, POM/BTZ, MEZI/DEX, MEZI/BTZ, or BTZ/DEX doublets, or the triplet combinations of POM/BTZ/DEX or MEZI/BTZ/DEX (see "Materials and methods" for dosing regimen). (A) Average tumor size over time for each cohort. (B) Statistical comparison (*t* test) of average tumor volume from each cohort in panel A on days 31, 38, 48, 52, and 57 after tumor inoculation for which red color indicates significance ($P < .05$) and blue, nonsignificance. (C) Individual mouse tumor size for either vehicle, or the triplet combinations of POM/BTZ/DEX or MEZI/BTZ/DEX are shown. (D) Kaplan-Meier survival curves and mOS is shown for all cohorts shown in panel A. (E) Statistical comparison (log-rank Mantel-Cox test) of survival curves from each cohort in panel C. NR, not reached.

Figure 4. Transcriptomic assessment by RNA sequencing of POM or MEZI triplet combinations with BTZ/DEX in H929 MM cells. (A) H929 MM cells were treated with either POM (100nM), MEZI (1nM), DEX (10nM), or BTZ (1-hour pulse, 50nM), or in triplet combinations for 24 hours followed by RNA sequencing and visualized with a heat map of DEGs. HALLMARK G2M CHECKPOINT and HALMARK E2F TARGET genes are denoted. (B) Gene set enrichment analysis (GSEA) of all HALLMARK pathways showing normalized enrichment scores from the indicated treatments (upregulated, red; downregulated, blue). (C) GSEA enrichment of the top upregulated and downregulated non-HALLMARK pathways comparing MEZI/BTZ/DEX vs POM/BTZ/DEX treatments. (D) Volcano plot of DEGs and those proteasomal subunit genes highlighted in the REACTOME_THE_ROLE_OF_GTSE1_IN_G2_M_PROGRESSION_AFTER_G2_CHECKPOINT annotated pathway comparing the triplet combination of MEZI/BTZ/DEX vs POM/BTZ/DEX. (E) chromatin immunoprecipitation with sequencing analysis showing Ikaros bound to the promoter/transcription start site of selected genes in panel D w/wo treatment with MEZI (1nM) for 24 hours. padj, adjusted *P* value.

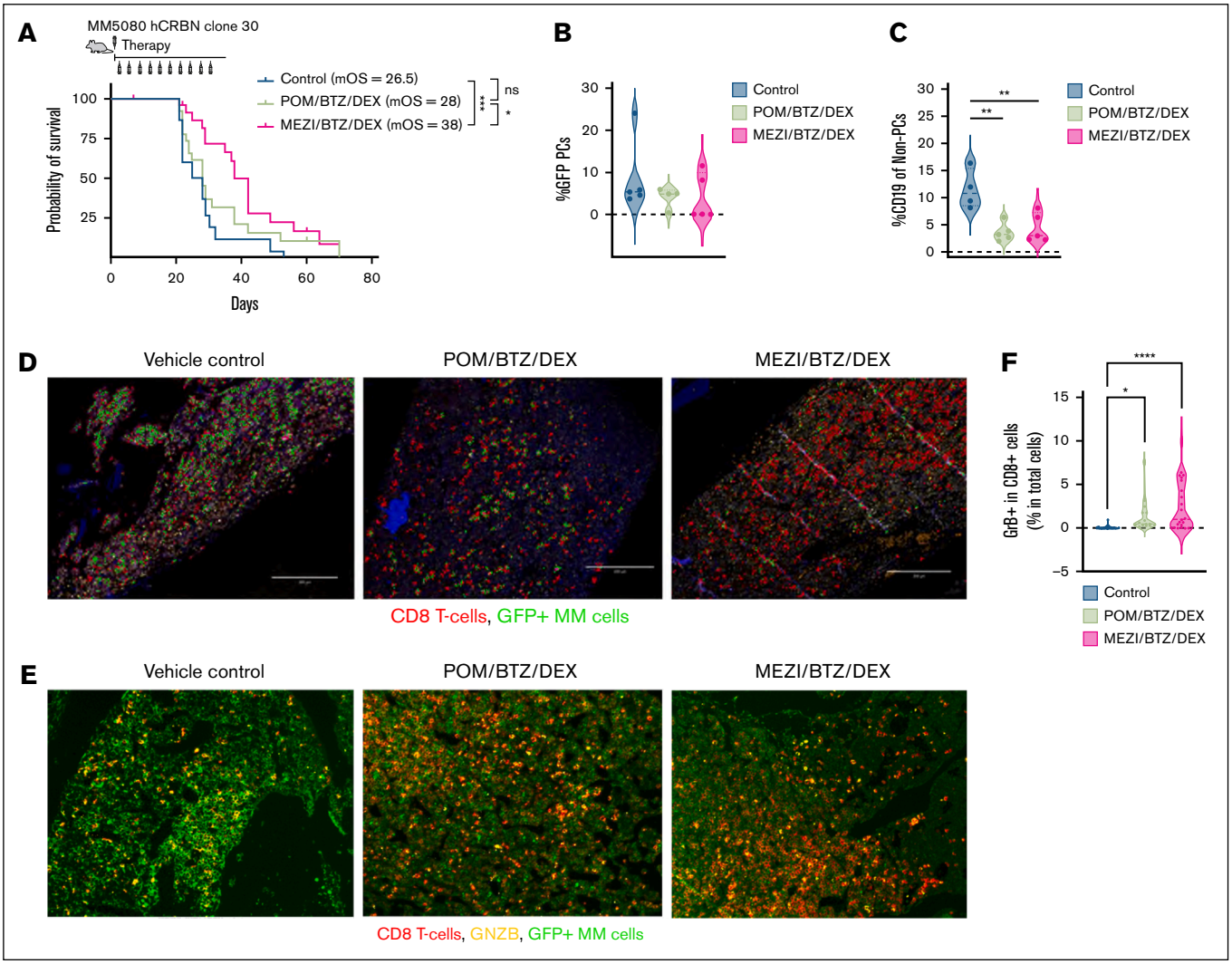

Figure 6. Evaluation of triplet combinations in a humanized CRBN syngeneic genetically engineered mouse model of MM. (A) Humanized *CRBN* mouse myeloma cells (MM5080^{CRBNI391V}, clone 30) were syngeneically engrafted into a humanized *CRBN* mouse followed by treatment with either vehicle control (n = 30), POM/BTZ/DEX (n = 27), or MEZI/BTZ/DEX (n = 27), and evaluated for survival efficacy, significance, and mOS (see "Materials and methods" for dosing regimen). (B-C) Flow cytometric quantification of percentage GFP$^+$ PCs or CD19$^+$ (percentage of gated live) MM5080^{CRBNI391V} cells isolated from femur bone marrow of mice in each cohort (n = 5) on day 22 of therapy. (D) Immunofluorescent staining and microscopic imaging of PC^{GFP+} (green), CD8$^+$ (red), and DNA (DAPI [4′,6-diamidino-2-phenylindole]; blue) localization determined by software-generated inference. (E) Immunofluorescent staining and microscopic imaging of PC^{GFP+} (green), CD8$^+$ (red), GZMB (yellow), and DNA (DAPI; blue). (F) Semiquantitative analysis of double-positive CD8$^+$/GZMB$^+$ cells for each condition in panel E. GNZB, granzyme B.

have demonstrated that the combinations of the drugs are synergistic.[8,10-12,41] This preclinical observation is confirmed by the pharmacodynamic assessment of Aiolos/Ikaros in B and T cells from the periphery of patients enrolled in ongoing MEZI clinical studies (with BTZ-containing cohorts), indicating that MEZI is still capable of degrading these substrates even during the coadministration of BTZ (Figure 7A-B). This is potentially explainable by their temporal dosing schedule within the clinic, in which MEZI (21-/28-day schedule) and BTZ is only coadministered on days 1, 4, 8, and 11, providing gaps in maximal proteasome inhibition allowing deep degradation of Aiolos/Ikaros substrates (Figure 7C). Secondly, these observations could also be accounted for by a nonoverlapping mechanism explaining their observed clinical synergy. CRBN-binding agents may function primarily by recruiting neomorphic substrates (eg, Aiolos/Ikaros) for polyubiquitination,[21,42-44] potentially rendering them inactive as transcriptional regulators. In this context, assay measurement of the reduction in overall substrate protein may not be an adequate assessment of the IMiD/CELMoD MOA in the presence of PIs rather than an indication of antagonizing MOAs.

Our findings demonstrate that MEZI induces more pronounced substrate degradation and cell cycle disruption compared with POM, consistent with its enhanced CRBN-binding affinity and ability to confer 100% "closed" active conformation.[4,22] We found that the MEZI/BTZ combinations conferred a rapid increase of cells in both G0/G1 and G2/M, including populations greater than tetraploid, potentially indicating mitotic slippage, although this is

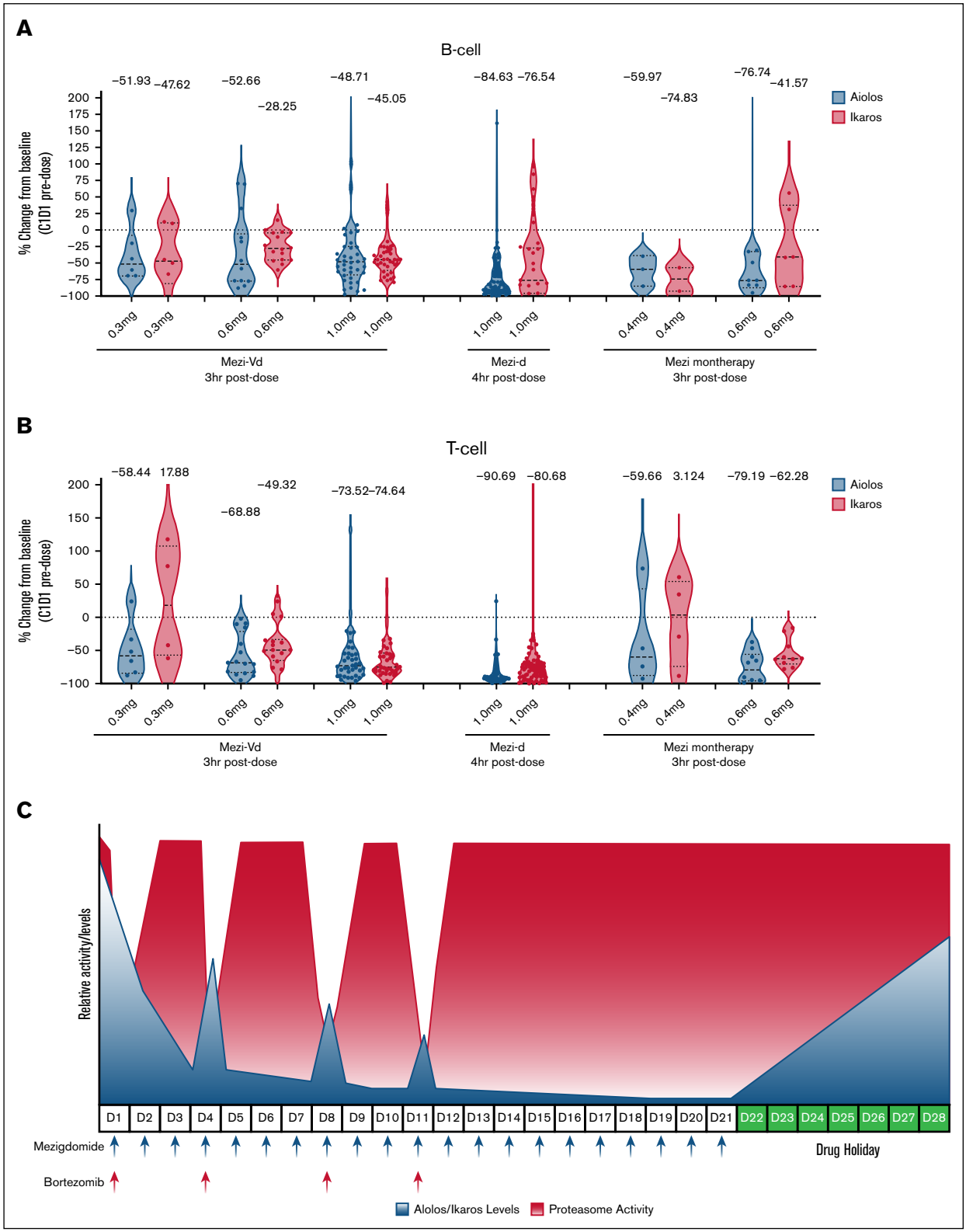

Figure 7. Changes in Aiolos and Ikaros in B and T cells from patients treated in MEZI clinical studies (ClinicalTrials.gov identifier: NCT03989414) and mechanistic model of overlapping MEZI/BTZ exposure/activity during therapy. Relative change (percentage change from baseline minus C1D1 before dose) in B cells (A) or T cells (B) from the peripheral blood of patients treated with either Mezi-Vd, Mezi-d, or MEZI single agent (Mezi monotherapy) on C1D1 after dose (3 or 4 hours). (C) Schematic of relative Aiolos/Ikaros degradation induced by MEZI (shaded blue) and the inhibition of the proteasome by BTZ (shaded red) in combination during 21-days of 28-day schedule of a single cycle (eg, first cycle). C1D1, cycle 1, day 1; Mezi-d, MEZI/DEX; Mezi-Vd, MEZI/BTZ/DEX.

hypothetical and not supported by the current evidence. Mechanistically, MEZI appears to work in concert with the G2/M-arresting mechanism previously demonstrated for BTZ, potentially due to simultaneous proteasome inhibition and downregulation of proteasome subunit expression by MEZI compared with POM. Because high proteasome activity is necessary for essential cell cycle protein degradation (eg, cyclins) for G2/M progression, the downregulation of proteasome subunit expression may result in a cooperative negative cell cycle effect with BTZ plus MEZI. As alluded to, it is not known whether the rapid ubiquitination of substrates is sufficient to impart the cytotoxic effects of CELMoD agents. However, if it is sufficient, MEZI's rapid ubiquitination/depletion of Aiolos/Ikaros, which can act in both activation and repressive complexes,[45] may be enough to disrupt G2/M progression in combination with BTZ via a rapid transcriptional effect on key protein complexes required for mitotic progression. However, the precise molecular drivers of G2/M arrest in this context remain incompletely defined.

The superior survival efficacy of the MEZI/BTZ/DEX triplet was highlighted within 2 different in vivo models of MM. However, significant differences in tumor clearance and OS were noted between these models. The tumor microenvironment, immune system compatibility, genetic and molecular profiles, and tumor heterogeneity differ between the xenograft and syngeneic models, leading to differences in tumor behavior, drug response, and disease progression. The immunocompromised xenograft model fails to represent the immune system's potential role in disease response and resistance. In contrast, the syngeneic model uses mouse MM cells that home to the bone marrow, closely mimicking the natural disease setting and allowing for interactions with immune components and the bone marrow niche. Additionally, the genetic and molecular differences between the human MM cell line xenograft and the syngeneic immunocompetent mice are distinct, potentially contributing to varying therapeutic outcomes. Despite these differences, the CELMoD triplet showed rapid and sustained tumor regression and improved survival in both models.

A limitation of this study is the reliance on established MM cell lines and engineered murine models. Although these systems offer valuable insights under controlled experimental conditions, they may not fully capture the complexity and heterogeneity of patient-derived disease. In particular, the absence of data from primary MM cells limits the immediate clinical translatability of our findings. In addition to the direct cytotoxic effects on MM cells, CELMoDs are known to exert immunomodulatory activity, which contributes to their therapeutic efficacy. In this study, we included an initial analysis of $CD8^+$ T-cells in the syngeneic model (Figure 6D-E), which revealed treatment-associated changes consistent with enhanced immune activation. We are also exploring separately the impact MEZI may have on the reinvigoration of exhausted T cells,[46] and that these immunologic effects are an important component of the overall MOA, even in the presence of PIs. Future studies will aim to integrate these data with functional assays and clinical correlates to better understand how CELMoDs modulate the tumor microenvironment and contribute to the pleiotropic antitumor effects.

Authorship

Contribution: C.C.B. and P.R.H. conceptualized/designed the study, contributed to the execution of data acquisition, analysis, and interpretation, and wrote and edited the manuscript; A.K.G. conceptualized/designed the study, contributed to the execution of data interpretation, and wrote and edited the manuscript; M.L. and H.C. contributed to the execution of data acquisition, analysis, and interpretation, and edited the manuscript; J.K., K.W., R.K.S., C.-C.H., S.L., J.Z., S.S., S.D., P.S., K.G., L.W., and N.S. contributed to the execution of data acquisition, analysis, and interpretation; M.A. and T.C. contributed to the execution of data analysis and interpretation, and edited the manuscript; P.G.R. and N.J.B. contributed study samples, and to data analysis and interpretation; and A.T. and J.A.M.-C. conceptualized/designed the study, contributed to the execution of data interpretation, and wrote and edited the manuscript.

Conflict-of-interest disclosure: C.C.B., J.K., N.S., C.-C.H., S.L., J.Z., L.W., M.A., H.C., K.G., T.C., P.R.H., A.T., and A.K.G. are current or former employees of Bristol Myers Squibb (BMS) and have equity ownership. J.A.M.-C. has received funding for research from BMS, Roche/Genentech, AstraZeneca, Janssen, K36 Therapeutics, Regeneron Pharmaceuticals, and Palleon; and is an employee and has equity ownership in MIMO Biosciences. The remaining authors declare no competing financial interests.

The current affiliation for N.S. is Frezent Biological Solutions Inc, New York, NY.

The current affiliation for K.W. is Tufts University, Boston, MA.

The current affiliation for A.T. is Nutfield Department of Orthopedics, Rheumatology and Musculoskelatal Sciences, Oxford University, Oxford, UK.

ORCID profiles: C.C.B., 0000-0002-5965-3263; C.-C.H., 0009-0003-4215-4884; T.T.C., 0000-0002-1690-8035; N.J.B., 0000-0001-7353-7034; A.T., 0000-0003-0415-1706; A.K.G., 0000-0001-5512-1625.

Correspondence: Chad C. Bjorklund, Translational Medicine, Bristol Myers Squibb, 556 Morris Ave, S7-A2, Summit, NJ 07901; email: chad.bjorklund@bms.com.

References

1. Richardson PG, Ocio E, Raje NS, et al. CC-92480, a potent, novel cereblon E3 ligase modulator (CELMoD) agent, in combination with dexamethasone (DEX) and bortezomib (BORT) in patients (pts) with relapsed/refractory multiple myeloma (RRMM): preliminary results from the phase 1/2 study CC-92480-MM-002. *Blood*. 2021;138(suppl 1):2731.
2. Richardson PG, Trudel S, Popat R, et al. Mezigdomide plus dexamethasone in relapsed and refractory multiple myeloma. *N Engl J Med*. 2023;389(11):1009-1022.
3. Elnair RA, Holstein SA. Evolution of treatment paradigms in newly diagnosed multiple myeloma. *Drugs*. 2021;81(7):825-840.

4. Hansen JD, Correa M, Nagy MA, et al. Discovery of CRBN E3 ligase modulator CC-92480 for the treatment of relapsed and refractory multiple myeloma. *J Med Chem*. 2020;63(13):6648-6676.
5. Lopez-Girona A, Havens CG, Lu G, et al. CC-92480 is a novel cereblon E3 ligase modulator with enhanced tumoricidal and immunomodulatory activity against sensitive and resistant multiple myeloma cells. *Blood*. 2019;134(suppl 1):1812.
6. Rajkumar SV, Kumar S. Multiple myeloma current treatment algorithms. *Blood Cancer J*. 2020;10(9):94.
7. van de Donk NWCJ, Pawlyn C, Yong KL. Multiple myeloma. *The Lancet*. 2021;397(10272):410-427.
8. Wong L, Narla RK, Leisten J, et al. CC-92480, a novel cereblon E3 ligase modulator, is synergistic with dexamethasone, bortezomib, and daratumumab in multiple myeloma. *Blood*. 2019;134(suppl 1):1815.
9. Raje N, Mateos MV, Iida S, Reece D. Clinical evidence for immune-based strategies in early-line multiple myeloma: current challenges in decision-making for subsequent therapy. *Blood Cancer J*. 2023;13(1):41.
10. Paludo J, Mikhael JR, LaPlant BR, et al. Pomalidomide, bortezomib, and dexamethasone for patients with relapsed lenalidomide-refractory multiple myeloma. *Blood*. 2017;130(10):1198-1204.
11. Richardson PG, Oriol A, Beksac M, et al. Pomalidomide, bortezomib, and dexamethasone for patients with relapsed or refractory multiple myeloma previously treated with lenalidomide (OPTIMISMM): a randomised, open-label, phase 3 trial. *Lancet Oncol*. 2019;20(6):781-794.
12. Katz M, Bjorklund CC, Thakurta A, Serbina N. Mechanistic insights of pomalidomide activity in combination with bortezomib and dexamethasone in multiple myeloma and immune cells. *Blood*. 2018;132(suppl 1):1934.
13. Rychak E, Mendy D, Shi T, et al. Pomalidomide in combination with dexamethasone results in synergistic anti-tumour responses in pre-clinical models of lenalidomide-resistant multiple myeloma. *Br J Haematol*. 2016;172(6):889-901.
14. Amatangelo M, Bjorklund CC, Hagner P, et al. P-230: preclinical and translational biomarker analysis to support further clinical development and dose optimization of mezigdomide (MEZI; CC-92480) in combination with either bortezomib or carfilzomib. *Clinical Lymphoma Myeloma and Leukemia*. 2022;22:S161-S162.
15. Bjorklund C, Amatangelo M, Chiu H, et al. Pre-clinical and clinical immunomodulatory effects of pomalidomide or CC-92480 in combination with bortezomib in multiple myeloma. *Blood*. 2021;138(suppl 1):1613.
16. Bjorklund C, Amatangelo M, Kang J, et al. CC-92480 enhances cell-autonomous cytotoxicity through blockade of G 2/M transition when combined with bortezomib/dexamethasone in pre-clinical multiple myeloma. *Blood*. 2021;138(suppl 1):2669.
17. Ito T, Ando H, Suzuki T, et al. Identification of a primary target of thalidomide teratogenicity. *Science*. 2010;327(5971):1345-1350.
18. Lopez-Girona A, Mendy D, Ito T, et al. Cereblon is a direct protein target for immunomodulatory and antiproliferative activities of lenalidomide and pomalidomide. *Leukemia*. 2012;26(11):2326-2335.
19. Zhu YX, Braggio E, Shi CX, et al. Cereblon expression is required for the antimyeloma activity of lenalidomide and pomalidomide. *Blood*. 2011; 118(18):4771-4779.
20. Bjorklund CC, Lu L, Kang J, et al. Rate of CRL4CRBN substrate Ikaros and Aiolos degradation underlies differential activity of lenalidomide and pomalidomide in multiple myeloma cells by regulation of c-Myc and IRF4. *Blood Cancer J*. 2015;5(10):e354.
21. Krönke J, Udeshi ND, Narla A, et al. Lenalidomide causes selective degradation of IKZF1 and IKZF3 in multiple myeloma cells. *Science*. 2014; 343(6168):301-305.
22. Watson ER, Novick S, Matyskiela ME, et al. Molecular glue CELMoD compounds are regulators of cereblon conformation. *Science*. 2022;378(6619): 549-553.
23. Chen D, Frezza M, Schmitt S, Kanwar J, Dou QP. Bortezomib as the first proteasome inhibitor anticancer drug: current status and future perspectives. *Curr Cancer Drug Targets*. 2011;11(3):239-253.
24. Moreau P, Richardson PG, Cavo M, et al. Proteasome inhibitors in multiple myeloma: 10 years later. *Blood*. 2012;120(5):947-959.
25. Berges C, Haberstock H, Fuchs D, et al. Proteasome inhibition suppresses essential immune functions of human CD4+ T cells. *Immunology*. 2008; 124(2):234-246.
26. Blanco B, Pérez-Simón JA, Sánchez-Abarca LI, et al. Bortezomib induces selective depletion of alloreactive T lymphocytes and decreases the production of Th1 cytokines. *Blood*. 2006;107(9):3575-3583.
27. Shi CX, Kortüm KM, Zhu YX, et al. Proteasome inhibitors block Ikaros degradation by lenalidomide in multiple myeloma. *Haematologica*. 2015;100(8): e315-e317.
28. Li Y, Kassir N, Wang X, Palmisano M, Zhou S. Population pharmacokinetics and exposure response analysis of pomalidomide in subjects with relapsed or refractory multiple myeloma from the novel combination treatment of pomalidomide, bortezomib, and low-dose dexamethasone. *J Clin Pharmacol*. 2020;60(8):1061-1075.
29. Schwartz R, Davidson T. Pharmacology, pharmacokinetics, and practical applications of bortezomib. *Oncology (Williston Park)*. 2004; 18(14 suppl 11):14-21.
30. Shabaneh TB, Downey SL, Goddard AL, et al. Molecular basis of differential sensitivity of myeloma cells to clinically relevant bolus treatment with bortezomib. *PLoS One*. 2013;8(2):e56132.
31. Besse A, Besse L, Kraus M, et al. Proteasome inhibition in multiple myeloma: head-to-head comparison of currently available proteasome inhibitors. *Cell Chem Biol*. 2019;26(3):340-351.e3.

32. Bjorklund CC, Kang J, Amatangelo M, et al. Iberdomide (CC-220) is a potent cereblon E3 ligase modulator with antitumor and immunostimulatory activities in lenalidomide- and pomalidomide-resistant multiple myeloma cells with dysregulated CRBN. *Leukemia*. 2020;34(4):1197-1201.

33. Gandhi AK, Kang J, Capone L, et al. Dexamethasone synergizes with lenalidomide to inhibit multiple myeloma tumor growth, but reduces lenalidomide-induced immunomodulation of T and NK cell function. *Curr Cancer Drug Targets*. 2010;10(2):155-167.

34. Verhelle D, Corral LG, Wong K, et al. Lenalidomide and CC-4047 inhibit the proliferation of malignant B cells while expanding normal CD34+ progenitor cells. *Cancer Res*. 2007;67(2):746-755.

35. Bae H, Go YH, Kwon T, Sung BJ, Cha HJ. A theoretical model for the cell cycle and drug induced cell cycle arrest of FUCCI systems with cell-to-cell variation during mitosis. *Pharm Res*. 2019;36(4):57.

36. Hu L, Li B, Chen G, et al. A novel M phase blocker, DCZ3301 enhances the sensitivity of bortezomib in resistant multiple myeloma through DNA damage and mitotic catastrophe. *J Exp Clin Cancer Res*. 2020;39(1):105.

37. Larrayoz M, Garcia-Barchino MJ, Celay J, et al. Preclinical models for prediction of immunotherapy outcomes and immune evasion mechanisms in genetically heterogeneous multiple myeloma. *Nat Med*. 2023;29(3):632-645.

38. Fink EC, McConkey M, Adams DN, et al. Crbn (I391V) is sufficient to confer in vivo sensitivity to thalidomide and its derivatives in mice. *Blood*. 2018;132(14):1535-1544.

39. Wang B, Duan J, Zhou L. The paradoxical pharmacological mechanisms of lenalidomide and bortezomib in the treatment of multiple myeloma. *Anticancer Drugs*. 2021;32(3):227-232.

40. Moreau P, Karamanesht II, Domnikova N, et al. Pharmacokinetic, pharmacodynamic and covariate analysis of subcutaneous versus intravenous administration of bortezomib in patients with relapsed multiple myeloma. *Clin Pharmacokinet*. 2012;51(12):823-829.

41. Mitsiades N, Mitsiades CS, Poulaki V, et al. Apoptotic signaling induced by immunomodulatory thalidomide analogs in human multiple myeloma cells: therapeutic implications. *Blood*. 2002;99(12):4525-4530.

42. Chamberlain PP, Lopez-Girona A, Miller K, et al. Structure of the human Cereblon-DDB1-lenalidomide complex reveals basis for responsiveness to thalidomide analogs. *Nat Struct Mol Biol*. 2014;21(9):803-809.

43. Gandhi AK, Kang J, Havens CG, et al. Immunomodulatory agents lenalidomide and pomalidomide co-stimulate T cells by inducing degradation of T cell repressors Ikaros and Aiolos via modulation of the E3 ubiquitin ligase complex CRL4(CRBN.). *Br J Haematol*. 2014;164(6):811-821.

44. Sievers QL, Petzold G, Bunker RD, et al. Defining the human C2H2 zinc finger degrome targeted by thalidomide analogs through CRBN. *Science*. 2018;362(6414):eaat0572.

45. Fan Y, Lu D. The Ikaros family of zinc-finger proteins. *Acta Pharm Sin B*. 2016;6:513-521.

46. Chiu H, Zhao J, Ortiz Estevez M, Hagner PR, Gandhi AK. Mezigdomide reverses T-cell exhaustion through degradation of Aiolos/Ikaros and reinvigoration of cytokine production pathways. *Blood*. 2023;142(suppl 1):335.